tvst

DOI: 10.1167/tvst.6.2.8

Article

The Effect of Retinal Melanin on Optical Coherence Tomography Images

Melissa A. Wilk[1,4], Alison L. Huckenpahler[1], Ross F. Collery[1], Brian A. Link[1], and Joseph Carroll[1–3]

[1] Department of Cell Biology, Neurobiology, & Anatomy, Medical College of Wisconsin, Milwaukee, WI, USA
[2] Department of Ophthalmology, Medical College of Wisconsin, Milwaukee, WI, USA
[3] Department of Biophysics, Medical College of Wisconsin, Milwaukee, WI, USA
[4] Current affiliation: HudsonAlpha Institute for Biotechnology, 601 Genome Way, Huntsville, AL, USA

Correspondence: Joseph Carroll, Eye Institute, Department of Ophthalmology, Medical College of Wisconsin, 925 N 87th St, Milwaukee, WI 53226-0509, USA. e-mail: jcarroll@mcw.edu

Received: 21 October 2016
Accepted: 13 February 2017
Published: 3 April 2017

Keywords: albinism; imaging; melanin; COT; retina; zebrafish

Citation: Wilk MA, Huckenpahler AL, Collery RF, Link BA, Carroll J. The effect of retinal melanin on optical coherence tomography images. Trans Vis Sci Tech. 2017;6(2):8, doi:10.1167/tvst.6.2.8

Purpose: We assessed the effect of melanin on the appearance of hyperreflective outer retinal bands in optical coherence tomography (OCT) images.

Methods: A total of 23 normal subjects and 51 patients with albinism were imaged using the Bioptigen high-resolution spectral-domain OCT. In addition, three wild type, three albino (*slc45a2*$^{b4/b4}$), and eight *tyrosinase* mosaic zebrafish were imaged with the hand-held Bioptigen Envisu R2200 OCT. To identify pigmented versus nonpigmented regions in the *tyrosinase* mosaic zebrafish, en face summed volume projections of the retinal pigment epithelium (RPE) were created from volume scans. Longitudinal reflectivity profiles were generated from B-scans to assess the width and maximum intensity of the RPE band in fish, or the presence of one or two RPE/Bruch's membrane (BrM) bands in humans.

Results: The foveal RPE/BrM appeared as two bands in 71% of locations in patients with albinism and 45% of locations in normal subjects ($P = 0.0003$). Pigmented zebrafish retinas had significantly greater RPE reflectance, and pigmented regions of mosaic zebrafish also had significantly broader RPE bands than all other groups.

Conclusions: The hyperreflective outer retinal bands in OCT images are highly variable in appearance. We showed that melanin is a major contributor to the intensity and width of the RPE band on OCT. One should use caution in extrapolating findings from OCT images of one or even a few individuals to define the absolute anatomic correlates of the hyperreflective outer retinal bands in OCT images.

Translational Relevance: Melanin affects the appearance of the outer retinal bands in OCT images. Use of animal models may help dissect the anatomic correlates of the complex reflective signals in OCT retinal images.

Introduction

Over the last two decades, optical coherence tomography (OCT) has become a routine tool in the assessment of retinal structure in research and clinical settings.[1] Its superior axial resolution makes it valuable in studying individual retinal layers, and implementation of summed volume projections can provide detailed, layer-specific en face images.[2–5] Despite its use, controversy remains regarding the anatomic origin of the hyperreflective signals corresponding to the photoreceptors and other outer retinal structures on OCT.

In particular, two main theories exist regarding the identity of the outer retinal hyperreflective bands. Spaide and Curcio noted the presence of three outer retinal hyperreflective bands at the fovea and four in the perifovea.[6] Based on a systematic model comparing OCT to histology, they proposed that the first (most anterior) hyperreflective band corresponds to the external limiting membrane (ELM). The second band appeared to correspond to the inner segment ellipsoid zone (ISe or EZ). The third band corresponded to the cone outer segment/contact cylinder, later termed the interdigitation zone (IZ) by the International Nomenclature for Optical Coherence

Tomography Panel.[7] At the fovea, this IZ is adjacent to the retinal pigment epithelium (RPE), accounting for the loss of a distinguishable third band, separate from the fourth, RPE-Bruch's membrane (BrM) band.

More recently, Jonnal et al.[8] used adaptive optics (AO)–OCT to image the retina with higher resolution. Their work suggests that the ellipsoid is too thick to produce the second band, and the band is more proximal to the outer segment than the ellipsoid, suggesting that the second band is, in fact the inner segment/outer segment junction, rather than the EZ. Additionally, while the term IZ is broadly correct, they suggest that the origin of the third hyperreflective band actually is the cone outer segment tips (COST). Imaging this region over time reveals a shift that likely corresponds to the shedding and renewal of the outer segment, further supporting the definition of the third band as the COST.[9] Cideciyan et al. (*IOVS* 2014;55;ARVO E-Abstract 3397), Srinivasan et al.,[10] and Lee et al.[11] likewise named the second and third bands inner segment/outer segment junction and COST, respectively, but between the COST and RPE was an additional peak in reflectance, which they termed the rod outer segment tips (ROST). Liu et al.[12] used averaged en face AO-OCT images to illuminate patterns within the ROST and RPE bands that are consistent with the organization of those mosaics, even differentiating individual RPE cells in three dimensions. Furthermore, Lee et al.[11] found another peak posterior to the RPE band that they proposed to be BrM.

Recent imaging studies in patients with albinism may offer valuable insight into the origin of some of the outer retinal bands. Specifically, our work has shown that patients with albinism have a high prevalence of a "split band" appearance of the outermost hyperreflective band, such that the RPE-BrM band appears as two separate bands.[13] This band appeared more posterior than the proposed ROST band seen by others. We postulated that the appearance of this band was the result of reduced melanin pigment and, thus, reduced light scattering, resulting in the ability to differentiate RPE from BrM.[13] However, there appear to be differences in the relative reflectance and thickness between the RPE and BrM bands between the normal subjects imaged by Lee et al.[11] and our patients with albinism,[13] perhaps suggesting a role for melanin in the appearance of the OCT images.

With the increased use of OCT in research and the clinic, it is critical that we understand the origins of the outer hyperreflective bands to understand the structural effects of disease. Given the variability in retinal melanin among individuals,[14,15] across retinal eccentricities,[14–20] and with age,[14–17,20,21] its effect on OCT may be important for accurate interpretation of these images. We used OCT in humans and zebrafish to better understand the role of melanin pigment in the appearance of the outer retina. Approaches like this will help to delineate the anatomic correlates of the controversial outer retinal bands.

Methods

Human Subjects

All human research was conducted in accordance with the Declaration of Helsinki and was approved by the Institutional Review Board at the Medical College of Wisconsin. Informed consent was obtained after explanation of the nature and possible consequences of the study. We analyzed images for 23 normal controls (previously described by Wilk et al.[22]; Table 1) and 51 patients with albinism (Table 2). All subjects had one eye dilated and cyclopleged using one drop each of phenylephrine hydrochloride (2.5%) and tropicamide (1%). JC_10269, who has albinism, underwent imaging of both eyes due to the presence of ocular melanosis in the right eye (causing a difference in retinal melanin between eyes; Supplemental Fig. 1).[23] An IOL Master (Carl Zeiss Meditec, Dublin, CA) was used to measure axial length, which was used for lateral scaling of OCT images as described previously.[24] Line scans were acquired using the Bioptigen high-resolution spectral-domain OCT (Bioptigen, Research Triangle Park, NC) and were nominally 6 or 7 mm (1000 A-scans/B-scan; 100-120 repeated B-scans). A subset of five controls subjects (JC_0007, JC_0616, JC_0677, JC_10121, and JC_10145) were reimaged and assessed to compare across time/imaging session.

Zebrafish

Zebrafish studies were approved by the Institutional Animal Care and Use Committee at the Medical College of Wisconsin and conducted in accordance with the ARVO Statement for the Use of Animals in Ophthalmic and Vision Research. Three strains of zebrafish were used: wild type (WT), albino (*slc45a2*$^{b4/b4}$), and *tyrosinase*-mosaic. Mosaic expression of tyrosinase was achieved through CRISPR/Cas9 gene editing techniques.[25,26] CRISPR guide RNA was synthesized to target exon 1 on the zebrafish *tyr* gene at the following sequence:

Table 1. Control subjects

Subject	Age	Sex	Race	Eye	Number of Peaks		
					Fovea	Nasal	Temporal
JC_0002	28	M	C	OD	1	2	2
JC_0007	37	M	C	OD	2	1	2
JC_0138	25	F	A	OD	2	2	1
JC_0200	26	M	C	OD	2	1	1
JC_0571	25	M	C	OD	2	2	2
JC_0616	23	M	C	OD	1	2	1
JC_0628	63	M	C	OD	1	2	1
JC_0629	67	F	C	OD	1	1	1
JC_0645	20	M	C	OD	2	2	2
JC_0654	25	F	C	OD	2	1	1
JC_0661	23	M	AA	OD	1	1	1
JC_0677	24	F	C	OD	1	1	2
JC_0692	40	M	C	OD	1	1	1
JC_0769	21	F	C	OD	1	2	1
JC_0878	8	F	C	OD	2	2	1
JC_0905	21	M	C	OD	1	1	2
JC_10119	22	M	A	OD	2	1	1
JC_10121	23	M	AA	OS	1	1	1
JC_10145	49	F	C	OD	1	1*	1
JC_10147	13	M	C	OS	2	2	1
JC_10311	62	M	C	OD	2	1	2
JC_10312	15	M	C	OS	2	2	2
JC_10329	22	M	C	OS	2	1	2

*Indicates values that differed between first and second trials.
A, Asian; AA, African American; C, Caucasian; H, Hispanic; ND, Not disclosed; OD, right eye, OS, left eye.

CCTCCCCAGAAGTCCTCCAGTCC (PAM site underlined). Guide RNA was coinjected with in vitro–transcribed *cas9* mRNA. The resultant fish have patches of melanin in regions of functioning tyrosinase, as well as patches of reduced or absent melanin in regions where *tyrosinase* was modified. This patchy appearance can be seen in the retina and throughout the body. Zebrafish were imaged with the hand-held Bioptigen Envisu R2200 OCT (Bioptigen) using a 12-mm telecentric lens for axial length measurements and a mouse retina probe for retinal imaging under light-adapted conditions. Axial length measurements were obtained as described previously[27] and used for lateral scaling as detailed by Huckenpahler et al.[2] Retinal volume scans were nominally 1.2 × 1.2 mm (1000 A-scans/B-scan; 500 B-scans). Line scans were nominally 1.2 mm (1000 A-scans/B-scan; 40 repeated B-scans). When possible, scans were acquired at the optic nerve head and four quadrants surrounding it. Both eyes were imaged for each fish except fish 10 and 12 (mosaic, left eye only).

Image Analysis

Optical coherence tomography line scans were registered and averaged as previously described to increase the signal-to-noise ratio.[28] The number of frames averaged varied across subjects (5–40), with fewer frames used in subjects with more severe nystagmus. For zebrafish, when possible, 40 frames were averaged, but occasionally breathing artifacts required exclusion of frames and fewer (15-20) B-scans were used. Zebrafish volumetric OCT scans were used to generate en face, summed volume projection images for the RPE layer to highlight the patterns in pigmentation using previously described Java software (Oracle Corporation, Redwood Shores, CA).[2,29] En face images for the optic nerve and four surrounding quadrants were aligned in Photoshop (Adobe Systems, San Jose, CA). Averaged line scans

Table 2. Patients with albinism

Subject	Age	Sex	Race	Eye	Number of Peaks		
					Fovea	Nasal	Temporal
AD_0063	32	M	C	OD	2	2	2
AD_0065	31	M	ND	OD	1	1	1
BB_10965	44	F	C	OS	2	2	2
DC_0831	7	M	C	OD	2	2	2
GS_10977	18	F	C	OD	2	1	2
GS_10979	17	M	C	OD	2	2	2
JC_0103	20	M	C	OD	1	2	1
JC_0125	28	M	ND	OD	1	1	2
JC_0131	20	M	ND	OD	2	1	2
JC_0140	11	M	ND	OD	2*	1	1
JC_0150	25	F	ND	OD	2	1	2
JC_0157	13	M	C	OD	1	1	1
JC_0170	16	F	C	OD	2	1	2
JC_0174	19	M	C	OS	2	2	2
JC_0421	24	F	C	OD	2	2	2
JC_0438	23	M	C	OD	2	2	2
JC_0456	17	M	AA	OD	2	1	2
JC_0459	21	F	ND	OD	1	2	2
JC_0492	28	F	C	OD	1	1*	1
JC_0493	21	F	C	OD	2	2	2
JC_0829	10	F	C	OD	2	1	2
JC_10042	6	F	C	OD	2	2	2
JC_10043	45	M	C	OD	1	2	2
JC_10061	28	M	AA	OD	2	2	2
JC_10068	10	M	ND	OS	1	2	2
JC_10073	23	F	A	OS	1	2	2
JC_10074	20	F	AA	OD	2	2	1
JC_10081	11	F	C	OS	2	1	1
JC_10092	22	F	C	OD	2	2	2
JC_10093	17	M	C	OD	2	2	2
JC_10192	6	F	C	OS	1	2	2
JC_10193	16	M	C	OD	2	2	2
JC_10227	18	F	C	OD	2	2	2
JC_10230	18	F	C	OS	1	2	1
JC_10269	6	F	C	OD	1	1	1
				OS	2	2	1
JC_10278	14	M	C	OD	2	2	2
JC_10279	12	M	A	OD	2	1	1
JC_10287	10	M	C	OD	2	2	2
JC_10319	53	F	C	OD	2	2	2
JC_10496	69	M	C	OD	2	2	2
JC_10508	37	F	C	OD	2	2	2
JC_10725	21	F	ND	OD	1	1	1
JC_10726	23	M	ND	OD	2	1	2
JC_10797	15	M	H,C	OD	2	2	2

Table 2. Continued.

Subject	Age	Sex	Race	Eye	Number of Peaks		
					Fovea	Nasal	Temporal
JC_10841	25	M	C	OS	2	2	2
JC_11046	37	M	C	OS	2	2	2
JC_6809	61	M	C	OD	2	2	1
KS_0551	31	M	C	OD	2	2	2
KS_0935	7	M	C	OD	2	2	2
KS_10314	5	F	C	OD	1	2	2
TC_10110	40	F	C	OS	2	1	1

*Indicates values that differed between first and second trials. A, Asian; AA, African American; C, Caucasian; H, Hispanic; ND, Not diclosed; OD, right eye; OS, left eye.

were matched to the corresponding B-scan within the volume to locate areas with and without melanin pigment from the en face image for subsequent analysis. Only line scans from the four quadrants (not the optic nerve) were used for analysis due to the size of the optic nerve.

To assess the appearance of the outer retinal bands, longitudinal reflectivity profiles (LRP) were generated using previously described Java (Oracle Corporation) software (OCT Reflectivity Analytics).[22] For zebrafish, LRPs were created for averaged B-scans in the linear format and averaged over an 11-pixel width in areas with no blood vessels (which cause blurring of the image). Noise reduction, which applies a median filter to the image (replacing each pixel in the image with the median pixel value of itself and its nearest neighbors), was used to decrease the noise of the image and subsequent LRPs.[22] A total of three to four LRPs were generated per eye in WT and albino fish, and twice as many were generated in *tyrosinase*-mosaic fish to capture areas with and without pigment. The full width at half maximum (FWHM) and maximum reflectance of the RPE were measured. Human subjects were analyzed for the presence of one or two RPE/BrM bands at the fovea and 1.5 mm nasal and temporal. Three LRPs were generated at each location, separated by 25 μm, using linear format images with OCT smoothing of 0.7 and averaging over a 5-pixel width. The reported number of RPE bands corresponds to the majority of measurements (two of three or three of three measurements) for each location. Peak identification in human LRPs was conducted by a single observer (MAW) and repeated. Any LRPs resulting in discordant peak number (1 versus 2) were repeated a third time, with the majority count being reported.

Histologic Comparison in Zebrafish

Following imaging, the zebrafish were anesthetized then decapitated and heads fixed in 4% paraformaldehyde overnight. Light-adapted eyes were removed from the head, and the anterior segment dissected from the eyecup. The eyecup was imaged from the scleral aspect. The en face OCT images were aligned to corresponding ex vivo images in Photoshop (Adobe Systems).

Statistical Analysis

Statistical comparisons were done using InStat (GraphPad, La Jolla, CA). Fisher's exact test was used to compare the number of RPE-BrM peaks between controls and patients with albinism for each of the three locations (fovea, nasal, and temporal). For zebrafish statistical comparisons, a single measurement corresponded to the peak reflectance (or FWHM) measured from a single LRP, with multiple LRPs (measurements) per eye. Kruskal-Wallis test was used to assess if any differences existed across zebrafish groups for peak reflectance and/or FWHM. Postanalysis was completed using Dunn's multiple comparisons test to determine pairwise differences across groups.

Results

Melanin Affects the Banding in Human OCT

The number of foveal and peripheral outer retinal peaks for each subject are given in Tables 1 and 2. Measurements showed excellent intragrader repeatability with only 1% of reported values differing between the two trials (asterisks in Tables 1 and 2). Of the 23 control subjects, 12 had two distinct RPE

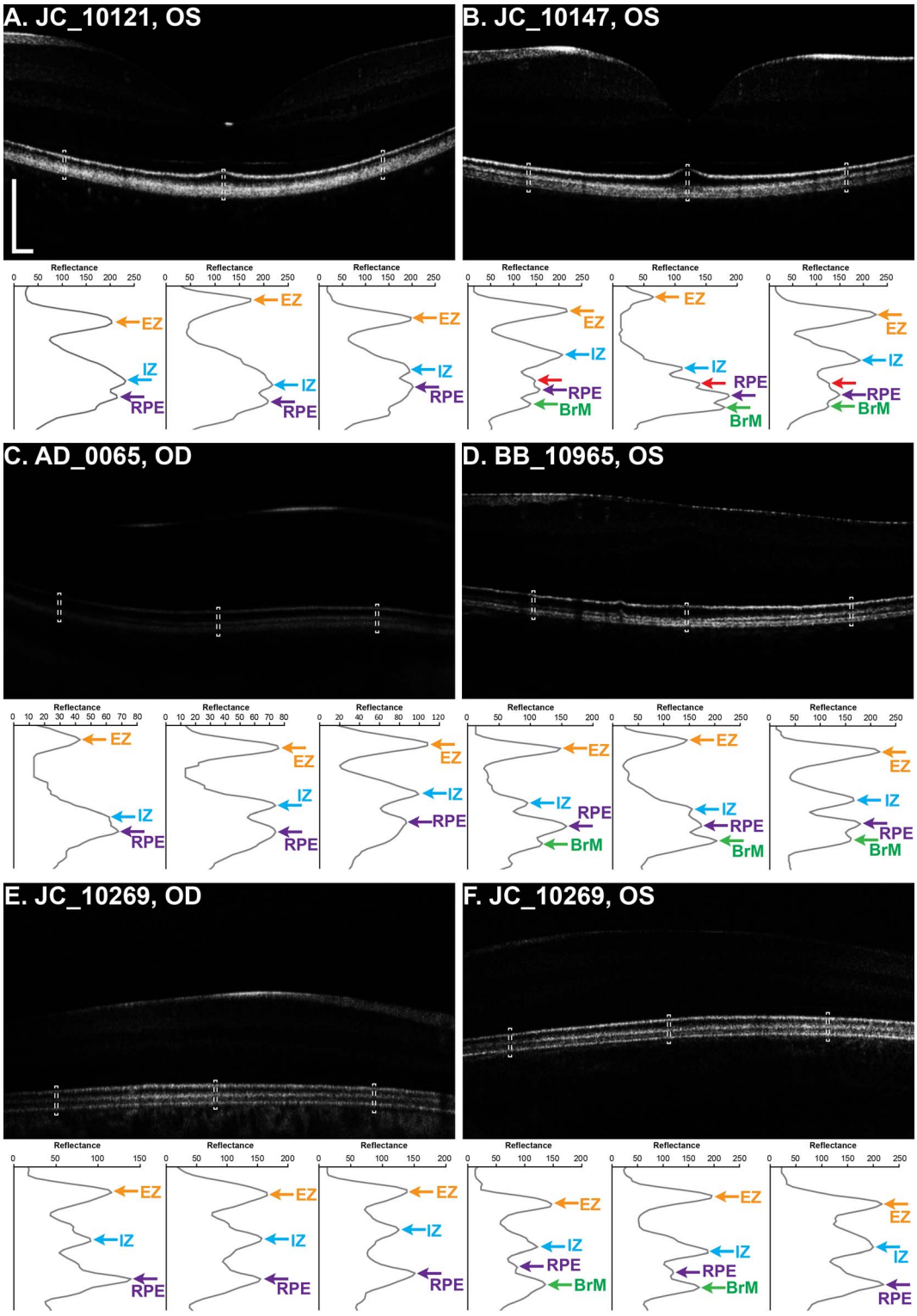

Figure 1. Outer retinal peaks in human OCT. Images are displayed in linear format with smoothing of 0.7 as used for analysis. (A) Normal subject with one peak for the RPE/BrM (*purple arrows*). (B) Normal subject with clear delineation of RPE (*purple arrow*) and BrM (*green arrow*) bands. An additional peak can be seen between the interdigitation zone (IZ) and RPE in the periphery, and presumably is the rod outer segments tips (ROST) (*red arrows*) due to its proximity to the RPE. Between the locations assessed (*white boxes* on the OCT image) are regions where the RPE/BrM appears as a single band. This phenomenon is seen commonly across subjects. (C) Patient with albinism

that lacks the split RPE/BrM. Due to nystagmus, averaging of B scans resulted in the IZ peak in reduction of the temporal retina. (D) Representative patient with albinism showing the distinct separation of RPE (*purple*) and BrM (*green*). (E–F) JC_10269, the patient with ocular melanosis of the right eye, shows a difference in number of peaks between eyes in the foveal and nasal retina only, and the peaks are more prominent in the less pigmented eye (*left eye*, [F]). Combined, these subjects highlight the variability in melanin and OCT appearance across normal subjects as well as patients with albinism. *Orange arrows*, ellipsoid zone (EZ); *blue arrows*, IZ; *red arrows*; presumed ROST; *purple arrows*, RPE; *green arrows*, BrM. *Scale bars*: 200 μm. *Dashed lines* in images denote the location of LRPs below. All LRPs, generated from the linear image with smoothing of 0.7, were over a 75-μm height and averaged over a 25-μm width, except the foveal LRPs for JC_10121 (83-μm height) and JC_10147 (98-μm height), who had greater elongation of foveal cone outer segments.

peaks in the fovea, 10 at 1.5 mm nasal, and 9 at 1.5 mm temporal (Figs. 1A, 1B). Only three of the 23 control subjects had an average of two peaks at all three locations (JC_0571, JC_0645, and JC_10312) while five subjects had a single peak at all locations (JC_0629, JC_0661, JC_0692, JC_10121, and JC_10145). For the five control subjects for which repeat imaging was done, only 53% of measurements were concordant across sessions, suggesting poor intersession repeatability despite high intragrader repeatability.

For foveal and temporal retina, 38 of 52 eyes from patients with albinism had two peaks, while 35 of 52 eyes had two peaks in the nasal retina (Figs. 1C–F). Five of these subjects had a single peak across all locations while 24 subjects with albinism had two peaks at all three locations. In JC_10269, the patient with ocular melanosis in the right eye, the more pigmented eye had a single peak at all locations while the less pigmented eye had two distinct peaks in the foveal and nasal retina. Overall, two distinct peaks were more likely to occur in patients with albinism than in control subjects (71% in albinism versus 45% in controls, $P = 0.003$; Fisher's exact test).

In addition, the peaks qualitatively appeared different between patients with albinism and normal controls. The peaks appeared more distinct in most of the patients with albinism and were persistent throughout the retina (Figs. 1D, 1F). Control subjects often had patches with two distinct peaks adjacent to areas with one peak (Fig. 1B). The two peaks also tended to be more distinct in peripheral retina than at the fovea. In JC_10269, the double peaks were present in the less pigmented eye and absent in the more pigmented eye. (Figs. 1E, 1F). Three control subjects and seven patients with albinism also had a peak between the IZ and RPE peaks (red arrow, Fig. 1B), which likely corresponds to the ROST.

Differences in RPE Peak Reflectance and Width in Zebrafish

Wild type fish showed normal pigmentation of the body and retina while albino fish were hypopigmented (Figs. 3A, 3B). Mosaic fish had unique external pigmentation that appeared striped (Figs. 3C, 3D). Patterns of pigmentation seen in the ex vivo retinas of these fish paralleled the RPE intensity patterns seen in en face OCT images, with lighter areas on OCT corresponding to areas containing melanin pigment (Figs. 3, 4). Areas lacking melanin display additional peaks posterior to the RPE in the LRPs (Fig. 4), which likely correspond to the visualization of sclera

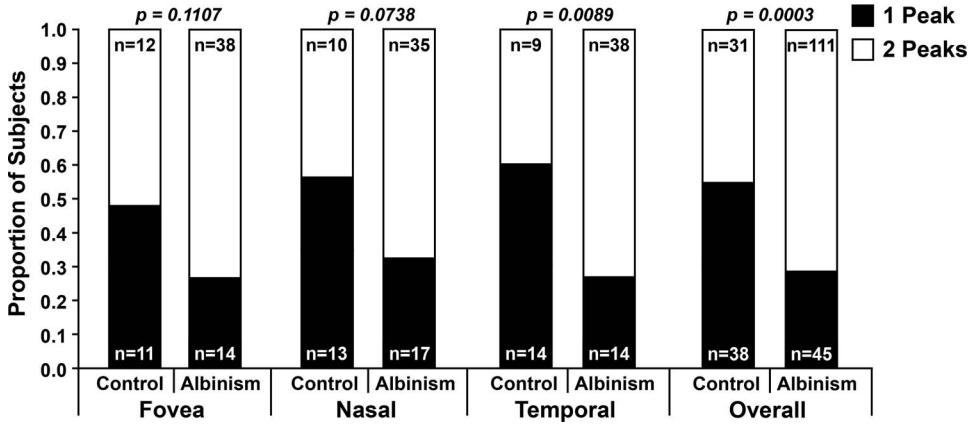

Figure 2. Differences in RPE-BrM peaks with melanin pigmentation. The presence of two peaks for RPE and BrM was more likely to occur in subjects with albinism than normal subjects. By individual location, only the temporal retina showed a significant difference.

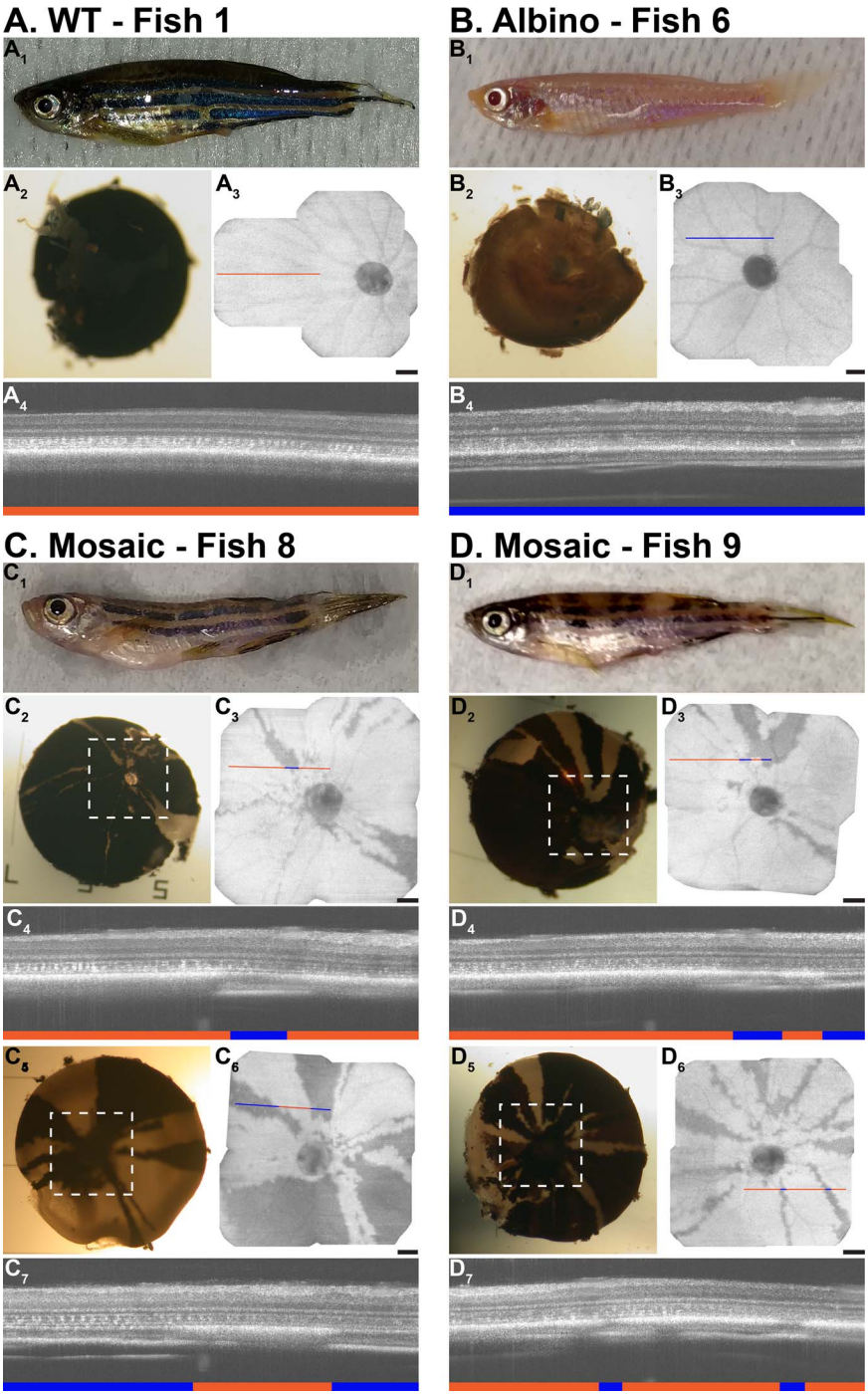

Figure 3. Pigmentation patterns of zebrafish strains. (A) WT zebrafish. (A_1) External pigmentation of normal zebrafish. (A_2) Ex vivo, posterior view of the normal eyecup. (A_3) En face OCT image from the same retina as (A_2). (A_4) In vivo cross-section of the retina at the location indicated by the orange line in (A_3). (B) Albino zebrafish. (B_1) External pigmentation of albino zebrafish. (B_2) Ex vivo, posterior view of the albino eyecup. (B_3) En face OCT image from the same retina as (B_2). (B_4) In vivo cross-section of the retina at the location indicated by the blue line in (B_3). (C–D) Two examples of mosaic zebrafish with unique pigmentation patterns. (C_1, D_1) External pigmentation of mosaic zebrafish. Retinal images from the right eyes (C_2–C_4, D_2–D_4) and left eyes (C_5–C_7, D_5–D_7) of two mosaic zebrafish. Posterior eyecups and en face OCT images show identical pigmentation patterns. *Dashed white boxes* on the eyecup denote the approximate location of the corresponding en face OCT images. For all fish, *lines* overlaid on the en face OCT mark the location of the B-scans below. *Orange lines* mark locations of melanin pigment while *blue lines* denote no pigment. Areas of pigment display bright RPE bands while areas lacking pigment have reduced RPE reflectance. The choroid and sclera are more visible in areas lacking pigment. *Scale bars*: 100 μm. All B-scans are 475 μm wide and tall and are displayed in the logarithmic format.

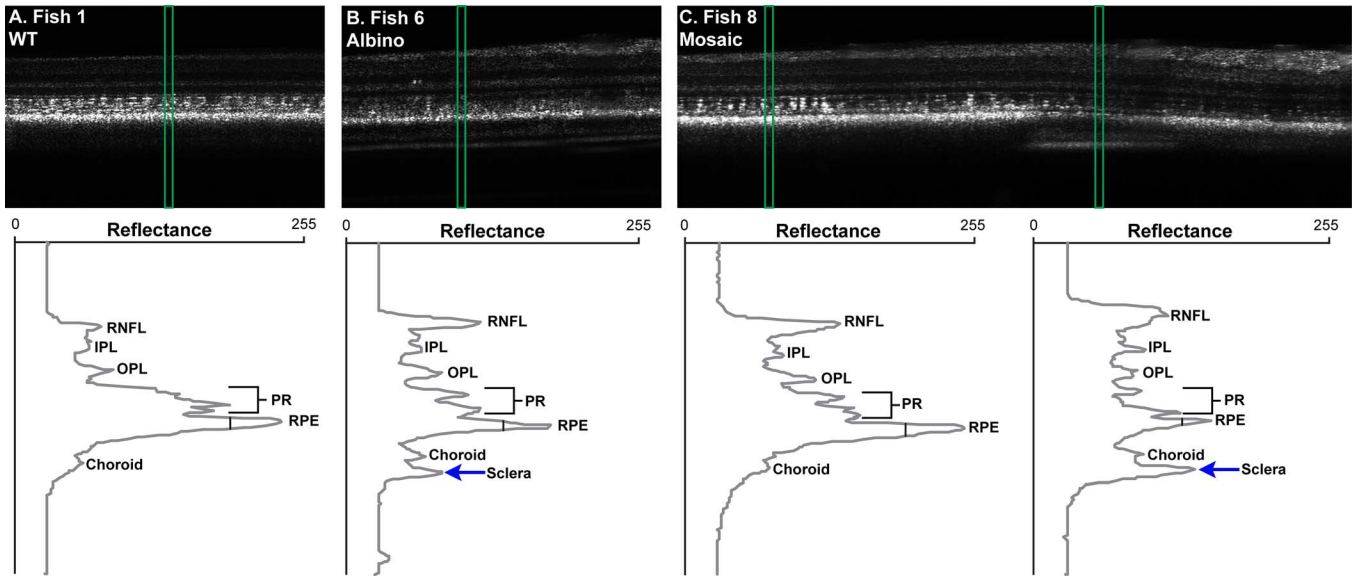

Figure 4. Differences in LRP peaks with pigmentation in zebrafish. (A) Wild type fish with consistent RPE reflectance and width. (B) Albino fish, whose RPE is distinctly dimmer than the WT. (C) Mosaic fish, where the left LRP was generated in an area with melanin pigment and the right LRP was generated in an area lacking pigment. When melanin in present, the RPE band is wider and has increased reflectance. When melanin is absent, the sclera also is visible posterior to the RPE and choroid. Wild type and albino images are 225 μm wide. Mosaic fish image is 475 μm wide. All images are 479 μm tall. Images are displayed in linear format with intensity values normalized to stretch between 0 and 255 for display only. RNFL, retinal nerve fiber layer; IPL, inner plexiform layer; OPL, outer plexiform layer; PR, photoreceptor layers.

in the absence of pigment. Quantitative results from zebrafish are summarized in Supplemental Table 1.

A total of 24 measurements of RPE reflectance and FWHM were taken in six WT eyes as well as 24 measurements in six albino eyes. For mosaic fish, 55 measurements were made in areas with melanin (pigment$^+$) across 14 eyes (8 fish), and 52 measurements were made in areas lacking melanin (pigment$^-$) across the same 14 eyes. When comparing peak RPE reflectance across groups, we found a significant difference ($P < 0.0001$; Kruskal-Wallis test). With Dunn's multiple comparisons test, we specifically found significant differences between WT and albino, WT and mosaic pigment$^-$, albino and mosaic pigment$^+$, and mosaic pigment$^+$ and pigment$^-$ ($P < 0.001$; Fig. 5A). There was no significant difference between albino and pigment$^-$, nor between WT and mosaic pigment$^+$ ($P > 0.05$). For the RPE FWHM, we also found a significant difference across groups ($P < 0.0001$; Kruskal-Wallis test). Specifically, there were significant differences between WT and mosaic pigment$^+$, albino and mosaic pigment$^+$, and mosaic pigment$^+$ and pigment$^-$ ($P < 0.001$; Dunn's multiple comparisons test; Figure 5B). There was no difference between WT and albino, WT and mosaic pigment$^-$, or albino and mosaic pigment$^-$ ($P > 0.05$). Measurements of reflectance and FWHM were averaged within each eye for each group. The averaged FWHM was plotted against the reflectance and found to have a significant correlation ($r_S = 0.63$, $P < 0.0001$; Spearman rank correlation), such that RPE bands with greater reflectivity tended to be wider as well (Fig. 5C). However, this relationship appears to be largely driven by the mosaic zebrafish.

Discussion

We examined the effect of melanin pigment on the appearance of images obtained with OCT using humans and zebrafish. The use of mosaic pigment zebrafish provides an internally controlled environment to examine differences due to pigment within a single retina. Through examination of genetically manipulated zebrafish in vivo and ex vivo, our data confirmed that disparities seen can be attributed to differences in melanin pigment, with the presence of melanin causing increased reflectance in the RPE that often broadens the band and impinges on adjacent bands (e.g., BrM), prohibiting their observation.[6] In patients with reduced or absent melanin pigment, the adjacent structures are seen more easily. While less distinct, these structures often are seen in normal

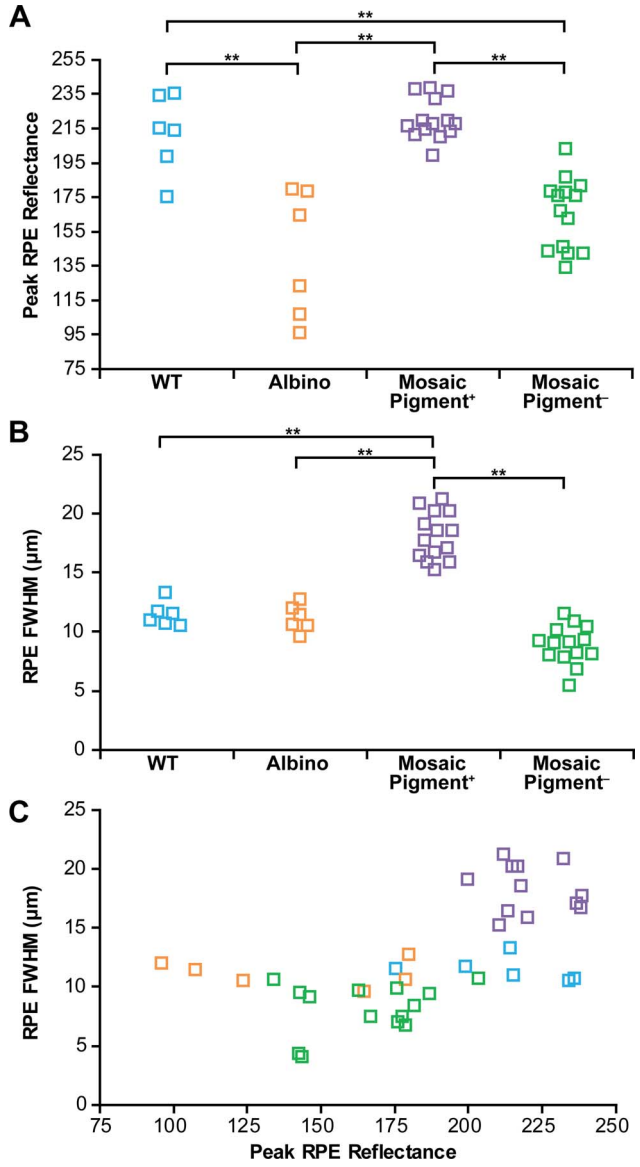

Figure 5. Differences in RPE reflectance and width with pigmentation in zebrafish. (A) Wild type zebrafish and pigment^{+} regions within mosaic zebrafish had significantly increased reflectance of the RPE than nonpigmented retinas. (B) Mosaic fish pigment^{+} regions had significantly wider RPE than all other fish and pigment^{-} regions of the same fish. (C) The FWHM was significantly correlated with RPE reflectance across fish, such that greater reflectance of the RPE corresponded to wider RPE. However, the relationship is driven by the mosaic fish. $^{**}p < 0.0001$.

subjects as well, perhaps suggesting that even differences in retinal melanin across normal individuals or within a given retina can alter the appearance of OCT images. In addition, the lack of agreement across imaging sessions within an individual highlights the importance of precise imaging. Differences seen in our subjects likely can be attributed to the subjective identification of the fovea and potential differences in exact imaging location or directionality of the OCT.[30] However, more work is needed to rule out other effects, such as time of day of imaging. These sources of disagreement suggest more comprehensive methods for analysis (e.g., volumetric analysis of OCT) may be less sensitive to local/regional variability in band appearance. Such analyses rely on accurate segmentation, which remains a major problem in OCT image analysis partly due to differences in device resolution, acquisition settings, and intersubject variability.

In zebrafish, significant differences in RPE peak reflectance were seen between retinas with and without pigment, regardless of genetic background. However, the differences seen in RPE width only exist between the mosaic pigment^{+} and other groups. While it is unsurprising that the pigment^{+} group is different from the albino and pigment^{-} groups, it is less clear why the pigmented regions of the mosaic fish RPE are similar in peak reflectivity but wider than WT retinas. It may be possible that the mosaic fish have altered light adaptation signaling, RPE morphology, and/or melanin migration that results in this difference. More work is needed to determine what aspects are altered and what is the underlying mechanism for the change.

Importantly, the presence or absence of melanin is not the only feature of the RPE pigment to consider for the appearance of OCT images. Previous studies have shown that melanosomes translocate within the RPE under different light conditions in several types of fish[31–34] and frogs.[35,36] In the dark, melanosomes are transported to the basal end of RPE cells. However, in light, melanosomes are moved into the apical projections of the RPE. Recently, Zhang et al.[35] used OCT to examine this phenomenon in frogs, showing an increase in the peak reflectance of the RPE band under dark-adapted conditions.[35] We assessed this phenomenon in a single WT zebrafish and found that the dark-adapted retina had a unique appearance when compared to the pigment-associated differences in RPE. With three hours of dark adaptation, the RPE band became more dispersed and granular, resulting in multiple, small peaks on the LRP. The relative location of the RPE band also appeared more posterior in the dark-adapted retina (Figs. 6A, 6C). In contrast, the light-adapted retina had a condensed, highly reflective RPE band adjacent to the photoreceptor layers (Figs. 6B, 6D). Since all other fish were imaged under light-adapted conditions, it is unsurprising that the light adapted RPE of

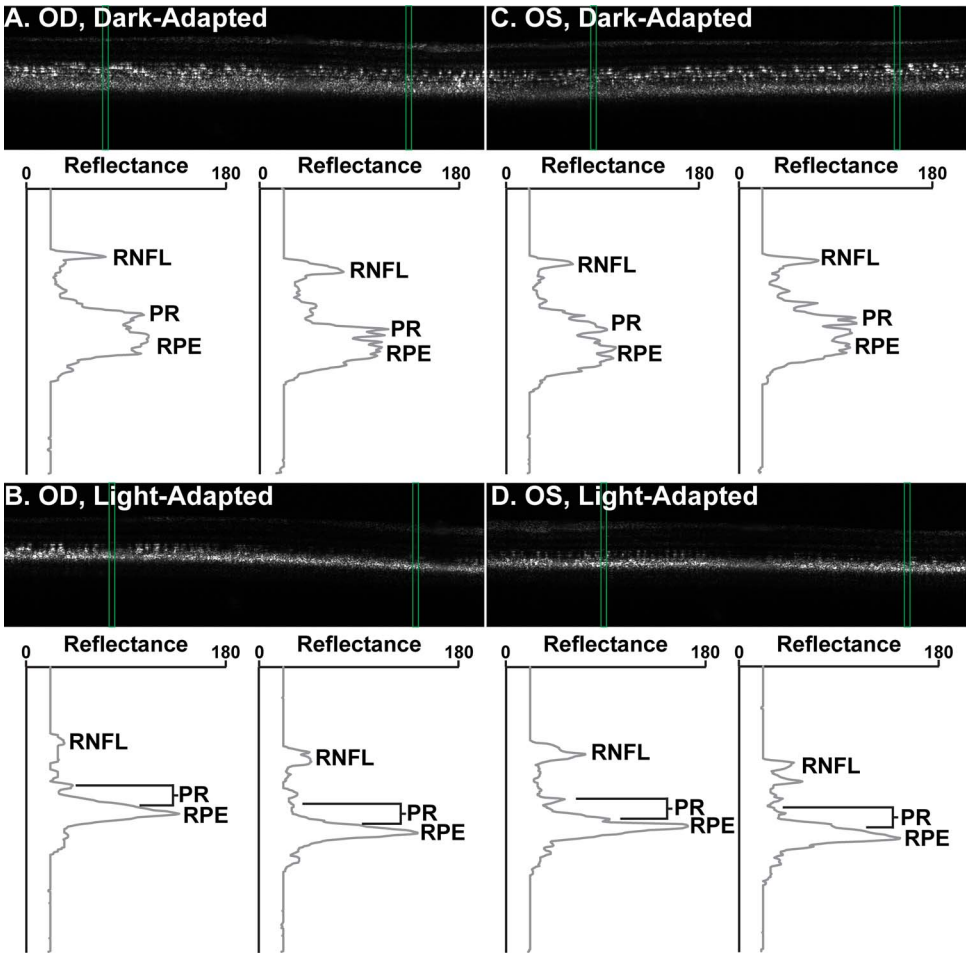

Figure 6. Light- and dark-adapted zebrafish OCT. *Green boxes* over images denote the location of the LRPs below. Right eye ([A]; OD) and left eye ([C]; OS) of WT zebrafish under dark adaptation. The RPE appears grainy and dispersed. Photoreceptor layers are distinct. (B, D) Corresponding light-adapted retinas. The RPE is more condensed and reflective. The RPE appears closer to the photoreceptor layers, which are much less distinct. Images are 475 μm wide and 479 μm tall. Images are displayed in linear format with intensity values normalized to stretch between 0 and 255 for display only.

this fish appeared similar to the WT fish examined above. These findings are consistent with the retinomotor movements described previously in zebrafish.[37]

Another interesting difference is that the dark-adapted retina presented clear photoreceptor layers while the light-adapted retina had a less distinct photoreceptor structure. This change could be due to changes in the intracellular milieu[38] or shortening of the photoreceptor outer segment[39] (increasing the distance between outer segment tips and RPE melanin) following light activation. Indeed, zebrafish have been shown to exhibit shortening of the rod outer segments and lengthening of cone outer segments with dark adaptation,[37] and Li et al.[40] also have shown outer segment shortening with dark adaptation in mice. In contrast, Abràmoff et al.[39] describe apparent outer segment shortening with light adaptation in humans. However, changes in appearance of the RPE band can affect segmentation algorithms designed to detect band edges.[41] As such, a broadening of the RPE band due to melanosome migration with light adaptation also could give rise to the apparent differences in outer segment "length." Alternatively, movement of melanin to basal RPE in dark conditions may reduce the interference of melanin with photoreceptor reflectivity. Under light-adapted conditions, the photoreceptor outer segments are surrounded by the pigment-containing processes of the RPE.[37] With dark adaptation, the pigment is displaced from the region of the the outer segments, which would allow better distinction of the outer segment regions from the RPE in OCT.[37] However, separation of photoreceptor bands and RPE is more

distinct in the light-adapted state compared to dark adaptation in mice.[40] As such, it is possible that in addition to changes in the amount of melanin pigment, the relative location and distribution of melanin within the RPE could affect the appearance of outer retina in OCT images, with differences across species.

While little work has been done to examine changes in normal human RPE with dark adaptation, several groups have used OCT to examine photoreceptor changes with dark adaptation in patients with Oguchi disease, a form of congenital night blindness due to defects in arrestin or rhodopsin kinase.[42–44] In these subjects, the peripheral outer segments appear normal (hyporeflective) when dark-adapted but increases in reflectance with light adaptation.[42–44] In addition to Oguchi disease, the presence of a tapetal-like reflex (TLR) in carriers of X-linked retinitis pigmentosa (XLRP) results in focal disruptions of the EZ,[45] which resemble the patterns of outer segment disruption noted by Takada et al.[43] in Oguchi patients. Examination of the underlying mechanisms and processes affected in patients with Oguchi disease and carriers of XLRP, as well as the changes associated with adaptation state, could provide key insight into the specific cellular structures regulating the reflectance of the outer retina.

The current accepted nomenclature as defined by the International Nomenclature for OCT Panel was developed based on three images from a single eye.[7] Moreover, the data presented to counter that nomenclature were obtained from four subjects (and no information about their retinal pigmentation status was provided).[8] However, our data highlight the tremendous variability in the appearance of the outer retina in OCT images across individuals and across images within an individual. Given such variability, clinicians and researchers should be careful extrapolating overarching theories from the OCT images of one or even a few individuals. To provide a thorough analysis of the anatomic correlates of OCT, all factors contributing to this variable appearance of these bands should be explored systematically, and controlled for when possible. As illustrated here, this could be accomplished using either animal models or by leveraging experiments of nature in human patients. Use of independent methods, such as near-infrared autofluorescence,[46,47] polarization sensitive OCT,[48,49] and photoacoustic ophthalmoscopy,[50,51] to measure retinal melanin may be worthwhile in future studies.

Acknowledgments

The authors would like to thank Robert Cooper, Erin Curran, Brian Higgins, Christopher Langlo, Erika Phillips, Edward Randerson, Moataz Razeen, Phyllis Summerfelt, and Erica Woertz for their contributions to this work. The authors also thank Gail Summers, Kimberly Stepien, Thomas Connor, Deborah Costakos, and Brian Brooks for patient referrals.

Supported by the National Eye Institute and the National Institute of General Medical Sciences of the National Institutes of Health under award numbers R01EY016060, R01EY024969, R01EY017607, T32EY014537, P30EY001931, and T32GM080202. This investigation was conducted in a facility constructed with support from Research Facilities Improvement Program, Grant Number C06RR016511, from the National Center for Research Resources, National Institutes of Health. The content is solely the responsibility of the authors and does not necessarily represent the official views of the National Institutes of Health. Additional support was provided by Vision for Tomorrow, The Edward N. & Della L. Thome Memorial Foundation, and an unrestricted departmental grant from Research to Prevent Blindness.

Disclosure: **M.A. Wilk**, None; **A.L. Huckenpahler**, None; **R.F. Collery**, None; **B.A. Link**, None; **J. Carroll**, None

References

1. Fujimoto J, Swanson E. The development, commercialization, and impact of optical coherence tomography. *Invest Ophthalmol Vis Sci*. 2016;57:1–13.
2. Huckenpahler AL, Wilk MA, Cooper RF, et al. Imaging the adult zebrafish cone mosaic using optical coherence tomography. *Vis Neurosci*. 2016;33:E011.
3. Scoles D, Flatter JA, Cooper RF, et al. Assessing photoreceptor structure associated with ellipsoid zone disruptions visualized with optical coherence tomography. *Retina*. 2016;36:91–103.
4. Rosen RB, Hathaway M, Rogers J, et al. Multidimensional en-face OCT imaging of the retina. *Opt Express*. 2009;17:4112–4133.

5. Sun LW, Johnson RD, Williams V, et al. Multimodal imaging of photoreceptor structure in choroideremia. *PLoS One*. 2016;11:e0167526.
6. Spaide RF, Curcio CA. Anatomical correlates to the bands seen in the outer retina by optical coherence tomography: Literature review and model. *Retina*. 2011;31:1609–1619.
7. Staurenghi G, Sadda S, Chakravarthy U, Spaide RF, Panel IO. Proposed lexicon for anatomic landmarks in normal posterior segment spectral-domain optical coherence tomography: The IN•OCT consensus. *Ophthalmology*. 2014;121: 1572–1578.
8. Jonnal RS, Kocaoglu OP, Zawadzki RJ, Lee SH, Werner JS, Miller DT. The cellular origins of the outer retinal bands in optical coherence tomography images. *Invest Ophthalmol Vis Sci*. 2014;55: 7904–7918.
9. Jonnal RS, Besecker JR, Derby JC, et al. Imaging outer segment renewal in living human cone photoreceptors. *Opt Express*. 2010;18:5257–5270.
10. Srinivasan VJ, Monson BK, Wojtkowski M, et al. Characterization of outer retinal morphology with high-speed, ultrahigh-resolution optical coherence tomography. *Invest Ophthalmol Vis Sci*. 2008;49:1571–1579.
11. Lee SH, Werner JS, Zawadzki RJ. Improved visualization of outer retinal morphology with aberration cancelling reflective optical design for adaptive optics - optical coherence tomography. *Biomed Opt Express*. 2013;4:2508–2517.
12. Liu Z, Kocaoglu OP, Miller DT. 3D imaging of retinal pigment epithelial cells in the living human retina. *Invest Ophthalmol Vis Sci*. 2016;57: OCT533-OCT543.
13. Wilk MA, McAllister JT, Cooper RF, et al. Relationship between foveal cone specialization and pit morphology in albinism. *Invest Ophthalmol Vis Sci*. 2014;55:4186–4198.
14. Weiter JJ, Delori FC, Wing GL, Fitch KA. Retinal pigment epithelial lipofuscin and melanin and choroidal melanin in human eyes. *Invest Ophthalmol Vis Sci*. 1986;27:145–152.
15. Feeney-Burns L, Hilderbrand ES, Eldridge S. Aging human RPE: Morphometric analysis of macular, equatorial, and peripheral cells. *Invest Ophthalmol Vis Sci*. 1984;25:195–200.
16. Schmidt SY, Peisch RD. Melanin concentration in normal human retinal pigment epithelium: Regional variation and age-related reduction. *Invest Ophthalmol Vis Sci*. 1986;27:1063–1067.
17. Boulton M, Dayhaw-Barker P. The role of the retinal pigment epithelium: Topographical variation and ageing changes. *Eye*. 2001;15:384–389.
18. Burke JM, Hjelmeland LM. Mosaicism of the retinal pigment epithelium: Seeing the small picture. *Mol Interv*. 2005;5:241–249.
19. Durairaj C, Chastain JE, Kompella UB. Intraocular distribution of melanin in human, monkey, rabbit, minipig and dog eyes. *Exp Eye Res*.2012; 98:23–27.
20. Hayasaka S. Aging changes in lipofuscin, lysosomes and melanin in the macular area of human retina and choroid. *Jpn J Ophthalmol*. 1989;33: 36–42.
21. Sarna T, Burke JM, Korytowski W, et al. Loss of melanin from human RPE with aging: Possible role of melanin photooxidation. *Exp Eye Res*. 2003;76:89–98.
22. Wilk MA, Wilk BM, Langlo CS, Cooper RF, Carroll J. Evaluating outer segment length as a surrogate measure of peak foveal cone density. *Vision Res*. 2017;130:57–66.
23. Radke P, Schimmenti LA, Schoonveld C, Bothun ED, Summers CG. The unique association of iris heterochromia with Hermansky-Pudlak syndrome. *J AAPOS*. 2013;17:542–544.
24. Wilk MA, Dubis AM, Cooper RF, Summerfelt P, Dubra A, Carroll J. Assessing the spatial relationships between fixation and foveal specializations. *Vision Res*. 2017;132:53–61.
25. Hwang WY, Fu Y, Reyon D, et al. Heritable and precise zebrafish genome editing using a CRISPR-Cas system. *PLoS One*. 2013;8:e68708.
26. Hwang WY, Fu Y, Reyon D, et al. Efficient genome editing in zebrafish using a CRISPR-Cas system. *Nat Biotechnol*. 2013;31:227–229.
27. Collery RF, Veth KN, Dubis AM, Carroll J, Link BA. Rapid, accurate, and noninvasive measurement of zebrafish axial length and other eye dimensions using SD-OCT allows longitudinal analysis of myopia and emmetropization. *PLoS One*. 2014;9:e110699.
28. Tanna H, Dubis AM, Ayub N, et al. Retinal imaging using commercial broadband optical coherence tomography. *Br J Ophthalmol*. 2010; 94:372–376.
29. Flatter JA, Cooper RF, Dubow MJ, et al. Outer retinal structure after closed-globe blunt ocular trauma. *Retina*. 2014;34:2133–2146.
30. Antony BJ, Stetson PF, Abramoff MD, et al. Characterizing the impact of off-axis scan acquisition on the reproducibility of total retinal thickness measurements in SDOCT volumes. *Transl Vis Sci Technol*. 2015;4:3.
31. Menger GJ, Koke JR, Cahill GM. Diurnal and circadian retinomotor movements in zebrafish. *Vis Neurosci*. 2005;22:203–209.

32. Braekevelt CR, Smith SA, Smith BJ. Fine structure of the retinal pigment epithelium of *Oreochromis niloticus* L. (Cichlidae; Teleostei) in light- and-dark adaptation. *Anat Rec*. 1998;252: 444–452.
33. Braekevelt CR. Circadian changes in the retinal pigment epithelium of the butterfly fish (*Pantodon buchholzi*). *Anat Anz*. 1990;171:284–292.
34. Burnside B, Adler R, O'Connor P. Retinomotor pigment migration in the teleost retinal pigment epithelium. I. Roles for actin and microtubules in pigment granule transport and cone movement. *Invest Ophthalmol Vis Sci*. 1983;24:1–15.
35. Zhang QX, Lu RW, Messinger JD, Curcio CA, Guarcello V, Yao XC. In vivo optical coherence tomography of light-driven melanosome translocation in retinal pigment epithelium. *Sci Rep*. 2013;3:2644.
36. Dearry A, Edelman JL, Miller S. Burnside B. Dopamine induces light-adaptive retinomotor movements in bullfrog cones via D2 receptors and in retinal pigment epithelium via D1 receptors. *J Neurochem*. 1990;54:1367–1378.
37. Hodel C, Neuhauss SC, Biehlmaier O. Time course and development of light adaptation processes in the outer zebrafish retina. *Anat Rec A Discov Mol Cell Evol Biol*. 2006;288:653–662.
38. Fain GL, Matthews HR, Cornwall MC, Koutalos Y. Adaptation in vertebrate photoreceptors. *Physiol Rev*. 2001;81:117–151.
39. Abràmoff MD, Mullins RF, Lee K, et al. Human photoreceptor outer segments shorten during light adaptation. *Invest Ophthalmol Vis Sci*. 2013;54:3721–3728.
40. Li Y, Fariss RN, Qian JW, Cohen ED, Qian H. Light-induced thickening of photoreceptor outer segment layer detected by ultra-high resolution OCT imaging. *Invest Ophthalmol Vis Sci*. 2016;57: OCT105-OCT111.
41. Stepien KE, Kay DB, Carroll J. Outer segment length in different best disease genotypes–reply. *JAMA Ophthalmol*. 2014;132:1153.
42. Godara P, Cooper RF, Sergouniotis PI, et al. Assessing retinal structure in complete congenital stationary night blindness and Oguchi disease. *Am J Ophthalmol*. 2012;154:987–1001.
43. Takada M, Otani A, Ogino K, Yoshimura N. Spectral-domain optical coherence tomography findings in the Mizuo-Nakamura phenomenon of Oguchi disease. *Retina*. 2011;31:626–628.
44. Yamada K, Motomura Y, Matsumoto CS, Shinoda K, Nakatsuka K. Optical coherence tomographic evaluation of the outer retinal architecture in Oguchi Disease. *Jpn J Ophthalmol*. 2009;53:449–451.
45. Acton JH, Greenberg JP, Greenstein VC, et al. Evaluation of multimodal imaging in carriers of X-linked retinitis pigmentosa. *Exp Eye Res*. 2013; 113:41–48.
46. Keilhauer CN, Delori FC. Near-infrared autofluorescence imaging of the fundus: Visualization of ocular melanin. *Invest Ophthalmol Vis Sci*. 2006;47:3556–3564.
47. Cideciyan AV, Swider M, Jacobson SG. Autofluorescence imaging with near-infrared excitation: Normalization by reflectance to reduce signal from choroidal fluorophores. *Invest Ophthalmol Vis Sci*. 2015;56:3393–3406.
48. Baumann B, Baumann SO, Konegger T, et al. Polarization sensitive optical coherence tomography of melanin provides intrinsic contrast based on depolarization. *Biomed Opt Express*. 2012;3: 1670–1683.
49. Schütze C, Ritter M, Blum R, et al. Retinal pigment epithelium findings in patients with albinism using wide-field polarization-sensitive optical coherence tomography. *Retina*. 2014;34: 2208–2217.
50. Zhang X, Zhang HF, Puliafito CA, Jiao S. Simultaneous in vivo imaging of melanin and lipofuscin in the retina with photoacoustic ophthalmoscopy and autofluorescence imaging. *J Biomed Opt*. 2011;16:080504.
51. Shu X, Liu W, Zhang HF. Monte Carlo investigation on quantifying the retinal pigment epithelium melanin concentration by photoacoustic ophthalmoscopy. *J Biomed Opt*. 2015; 20:106005.